Atmospheric Research 153 (2015) 437–450

Contents lists available at ScienceDirect

Atmospheric Research

journal homepage: www.elsevier.com/locate/atmos

Temporal characteristics of atmospheric CO_2 in urban Nanjing, China

Xiaoxian Huang [a], Tijian Wang [a,*], Robert Talbot [b], Min Xie [a], Huiting Mao [c], Shu Li [a], Bingliang Zhuang [a], Xiuqun Yang [a], Congbin Fu [a], Jialei Zhu [a], Xing Huang [a], Runying Xu [d]

[a] School of Atmospheric Sciences, Nanjing University, Nanjing 210093, China
[b] Department of Earth & Atmospheric Sciences, University of Houston, Houston, TX 77204, USA
[c] Department of Chemistry, State University of New York College of Environmental Science and Forestry, Syracuse, NY 13210, USA
[d] State Key Laboratory of Pollution Control and Resource Reuse, School of the Environment, Nanjing University, Nanjing 210023, China

ARTICLE INFO

Article history:
Received 22 May 2014
Received in revised form 22 August 2014
Accepted 23 September 2014
Available online 2 October 2014

Keywords:
Atmospheric carbon dioxide (CO_2)
Urban Nanjing
Traffic emissions
Firework settings
The CO_2/CO ratio

ABSTRACT

Although China is a big carbon dioxide (CO_2) emitter, in situ measurements of atmospheric CO_2 are sparse in urban China. The mixing ratio of carbon dioxide (CO_2) and its influencing factors in urban Nanjing were investigated in this study, from the 18th of January to the 31st of December 2011. The annual average mixing ratio of CO_2 was 406.5 ± 20.0 ppmv over the study period. The signal analysis using the fast Fourier transform (FFT) algorithm showed that CO_2 had different cycles as a result of multiple controlling factors. The seasonal and intra-seasonal fluctuations of CO_2 were mainly caused by the terrestrial biospheric uptake and emission and atmospheric oscillation. The weekly variation of CO_2 was largely influenced by traffic volume. The diurnal cycle of CO_2 presented a bimodal pattern in winter (DJF) probably due to the rush hour emissions. The seasonal mean CO_2/CO correlation slope varied from 0.024 ppmv/ppbv to 0.029 ppmv/ppbv, comparable to the fossil fuel combustion emission ratio. The diurnal pattern of CO_2/CO was irregular, indicating random anthropogenic emissions in an urban area. Firework setting was a large source of CO_2 during the Spring Festival holiday. The backward trajectories by the HYSPLIT model showed that the local anthropogenic emissions contributed the most to the high CO_2 mixing ratio in the urban area.

1. Introduction

Carbon dioxide (CO_2) is an important trace gas from the standpoint of climate change. It has a strong "greenhouse effect" and its global radiative forcing is increasing to 1.846 W m^{-2} in 2012 (Butler and Montzka, 2013). The annual average level of global background CO_2 measured at Mauna Loa Observatory is continuing to increase and currently is at 396.48 ppmv in 2013 (Tans and Keeling, 2014). The growth rates at different stations in the Northern Hemisphere have varied at around 1–3 ppmv over the past decade (Ferrarese et al., 2002; Nasrallah et al., 2003; Tsutsumi et al., 2006; Artuso et al., 2009; Hofmann et al., 2009; Wang et al., 2010b; Tans and Keeling, 2014). The global carbon cycle includes an exchange among the atmosphere, hydrosphere, biosphere, pedosphere, and geosphere (Finlayson-Pitts and Pitts, 2000). Anthropogenic activity has contributed to atmospheric CO_2 over the past two centuries. The preindustrial land use changes (LUC) have legacy effects on today's CO_2 by causing emissions (Pongratz and Caldeira, 2012) and remain the second largest source after the Industrial Revolution (Houghton, 2010; Houghton et al., 2012). During the industrial era, emissions from the consumption of fossil fuels and cement production act as the crucial source with a global estimation of 337 Gt C, half of which occurred in the past two decades (Boden et al., 2010).

In contrast to the study on background CO_2 levels, with emphasis on the circulation influences and relevant sources

* Corresponding author. Tel.: +86 25 83593797.
E-mail address: tjwang@nju.edu.cn (T. Wang).

http://dx.doi.org/10.1016/j.atmosres.2014.09.007
0169-8095/

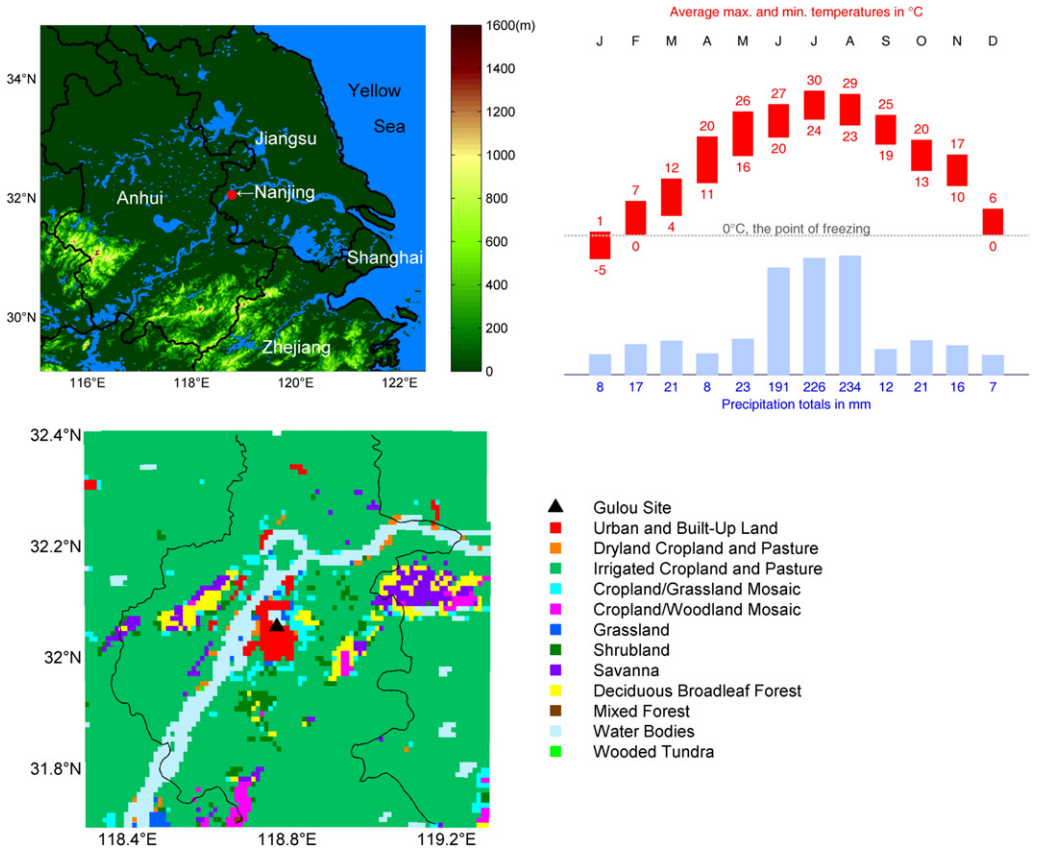

Fig. 1. Topography height (m) and land use distribution over Nanjing and vicinal areas with the location of the Gulou Site (32°3′20″N, 118°46′29″E), monthly precipitation totals (mm) and average maximum and minimum temperatures (°C) in Nanjing over 2011.

and sinks on a large scale (Keeling et al., 1976; Ferrarese et al., 2002; Tsutsumi et al., 2006; Zhang et al., 2013), the objectives of observations in (sub)urban and rural areas have been focused on the fundamental issues on the regional scale (e.g. Idso et al, 2001; Miyaoka et al., 2007; Pérez et al., 2009, 2011; Song and Wang, 2012). The growth and decay of vegetation affect urban CO_2 variations on annual to diurnal cycles (Nasrallah et al., 2003; Miyaoka et al., 2007; Gorka and Lewicka-Szczebak, 2013).

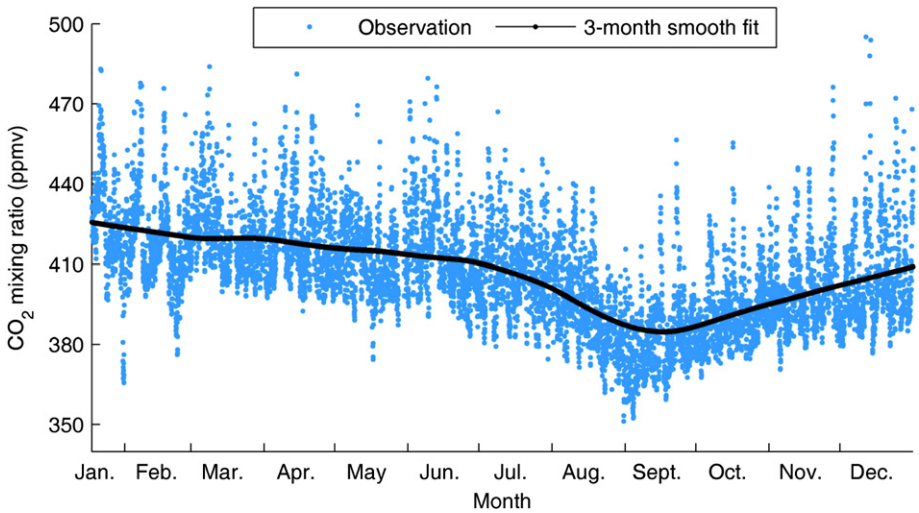

Fig. 2. Time series of hourly CO_2 mixing ratio (ppmv) observed at the Gulou Site in Nanjing over 2011. The black line stands for a 3-month smooth fit.

Besides the driving forces from the natural ecosystems, anthropogenic emissions from humans and automobile activity play have important roles in CO_2 variations (Idso et al., 2002; Gratani and Varone, 2005; García et al., 2012; Gorka and Lewicka-Szczebak, 2013). Affected by the urbanization processes, the results from the multi-point sampling suggest that spatial variations of different types of land utilization determine the distribution of CO_2 within the urban canopy layer (Idso et al, 2001; Henninger and Kuttler, 2010; Sahay and Ghosh, 2013; Gorka and Lewicka-Szczebak, 2013).

However, research on atmospheric CO_2 in China is limited (Wang et al., 2010b; Jiang et al., 2013; Zhang et al., 2013), especially in urban areas. With the aim of enhancing current knowledge on CO_2 variations, an urban air quality station began operating in Nanjing in January 2011. Nanjing is an inland city about 300 km away from the sea, with an area of 6600 km^2, a population of 8.2 million and about 1.8 million automobiles, representative of megacities in the Yangtze River Delta (YRD) region. The YRD, covering the alluvial plains surrounding the Yangtze River estuary, is a densely populated metropolitan area in China. As the center of Chinese economic development, the YRD is heavily industrialized and urbanized (Liao et al., 2014). However, available information remains scarce, thus the influence of possible sources and sinks on CO_2 variation in this area is still unknown.

In this paper, continuous measurements of atmospheric CO_2 were carried out in urban Nanjing throughout 2011. The goal of this study is to show the experimental results from multiple perspectives. The specific objectives are as follows: (1) to have a basic knowledge about the characteristics of atmospheric CO_2 in an urban area, (2) to explore the possible sources and sinks through the comparison with controlling factors, and (3) to estimate the anthropogenic emissions. The results may be of great help for the government in making energy conservation and emission reduction strategies and in estimating the anthropogenic emission inventory as well.

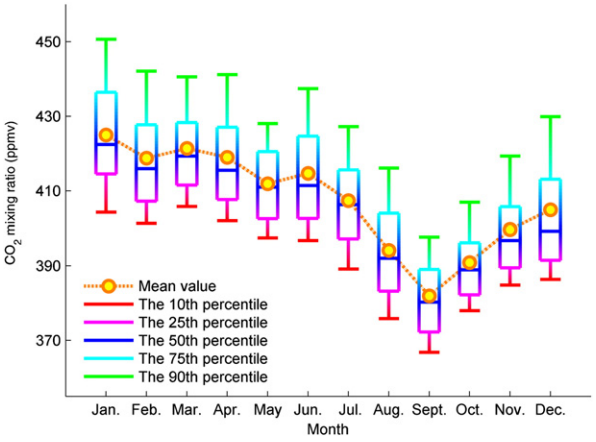

Fig. 4. Monthly variation of CO_2 mixing ratio with the mean values and the 10th, 25th, 50th, 75th, and 90th percentiles at the Gulou Site in Nanjing over 2011.

2. Experimental methodologies

2.1. Site description

Continuous atmospheric CO_2 and CO mixing ratios were observed on the roof of a 24-story building (32°3′20″N, 118°46′29″E) on the Gulou Campus at Nanjing University from the 18th of January to the 31st of December 2011. Simultaneous PM_{10} and $PM_{2.5}$ concentrations and meteorological parameters including relative humidity, air temperature, and air pressure were measured at the Gulou Site. Concurrent air quality indicators including NO_x (NO and NO_2), SO_2, and solar radiation were carried out at the Caochangmen Site (32°3′26″N, 118°44′55″E) of Nanjing Environmental Protection Agency, which is 2.3 km away from the Gulou Site. Both Gulou and Caochangmen sites are located in urban areas. Wind speed, wind direction and

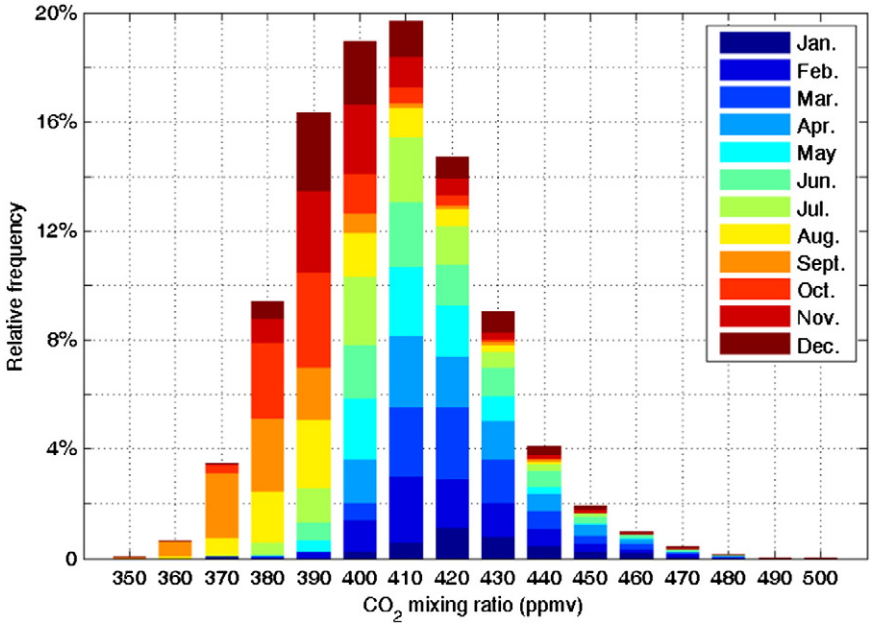

Fig. 3. Frequency distribution of hourly CO_2 mixing ratio (ppmv) at the Gulou Site in Nanjing over 2011.

precipitation were provided by the National Meteorological Station of Nanjing (ID 58238, 31°55′55″N, 118°53′59″E). The heavily populated area of Nanjing is about 750 km^2. The surrounding area outside the urban area is characterized by an agricultural field with sparse savanna and deciduous broadleaf vegetation (Fig. 1).

2.2. Measurements and data processing

The instrument used for the measurements of CO_2 was LI-COR LI-7000 differential non-dispersive infrared (NDIR) analyzer operated in a manner identical to that described by Talbot et al., 2005. It's a real-time trace gas monitor and is capable of measuring gases at high sensitivity. The sampling intake was installed 3.5 m above the roof level which was at a height of 80 m. The instrument sampled the air through a Teflon tube. Water vapor was removed through a chemical desiccant column and Nafion driers. Then the air sample was introduced to the NDIR analyzer. The data were continuously recorded on a 1-min scale and processed as hourly mean values. The instrument was automatically zeroed with Ultra High Purity Nitrogen every 12 h and calibrated every 14 h with calibration standards of 394 ppmv with a precision of 0.1 ppmv. Measurements of CO were made with a 1-minute time resolution using a Thermo Model 48i-TLE CO Analyzer (Mao and Talbot, 2004) and processed as hourly mean values as well. Before processing the 1-min data into hourly mean values, manual inspection was needed including the removal of the absent and abnormal values and the calibration of the measurements.

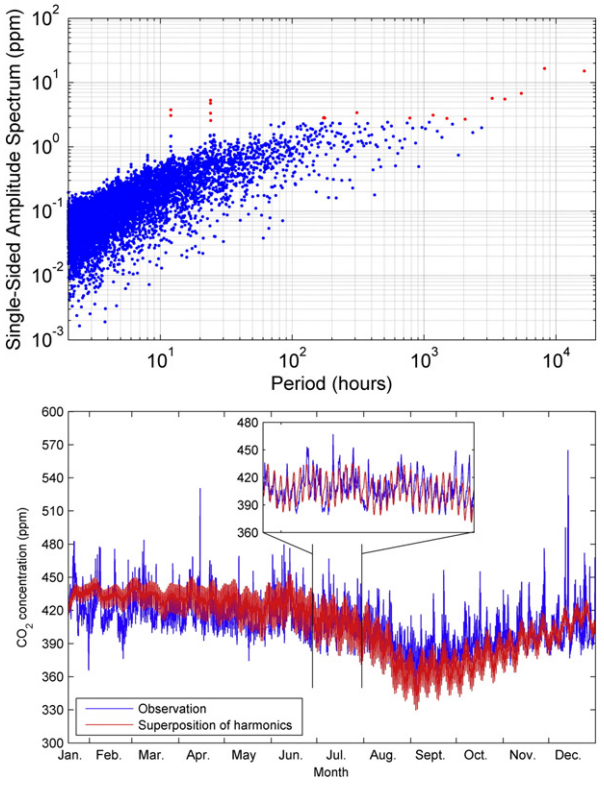

Fig. 5. Power spectrum of hourly CO_2 mixing ratio observed over 2011 at the Gulou Site in Nanjing. The red dots stand for the significant 19 harmonics with single-sided amplitude spectrums larger than 2.5 ppmv. The comparison between the observation and the superposition of harmonics.

2.3. Climate and microclimate

Nanjing has a subtropical monsoon climate with four distinct seasons. Summers are especially hot and rainy, while winters are relatively cold (Fig. 1). The annual average temperature over 2011 in urban Nanjing was about 15 °C, with monthly maximum values over 30 °C from May to September, and monthly minimum values below 0 °C from January to March and December. Annual precipitation was 782.3 mm in 2011. Monthly precipitation totals were extremely high from June to August, around 200 mm, while normally below 30 mm in other months. Mean wind speed was 1.8 m s^{-1} and wind directions were mainly east and east-southeast.

2.4. Other data sources

The NDVI derived from satellite measurements is widely used to estimate the density of the plant canopies. The NDVI of Level 3 data products V01.00 is generated by Thermal And Near-infrared Sensor for carbon Observation-Cloud and Aerosol Imager (TANSO-CAI) onboard Greenhouse gases Observing SATellite (GOSAT) provided by JAXA/NIES/MOE. The interval lengths of latitude and longitude are both 1/30°. The data is calculated for the 30 days, generated every 3 days, and shifted every 3 days. The median day among the 30 days was chosen to stand for the date of the 30-day product. The NDVI ranges from negative values to 1. Free standing water results in negative values while exposed soils tend to generate small positive values. A density vegetation canopy tends to show a value larger than 0.3. The vehicular information was obtained from the Nanjing Vehicular Emission and Pollution Monitoring and Management Center. The traffic emission inventory was estimated according to Wang et al. (2010a). The 5-day backward trajectories of air parcels were calculated and clustered by the HYSPLIT model of NOAA Air Resources Laboratory (Draxler and Rolph, 2013; Rolph, 2013) every 6 h during the study period with 2.5° × 2.5° resolution meteorological data.

3. Results and discussions

3.1. Overall description

Fig. 2 presents the time series of hourly CO_2 mixing ratio over the measurement period from the 18th of January to the 31st of December 2011. The atmospheric CO_2 shows a mean yearly value of 406.5 ppmv with a standard error of 20.0 ppmv. 99.9% of the 8176 available points range from 350 ppmv to 490 ppmv with only a few points over 500 ppmv. There is a strong seasonal cycle with a well-defined minimum at the beginning of September.

The frequency distribution of hourly CO_2 levels at each 10-ppmv interval is shown in Fig. 3. The most frequent levels were observed in the intervals from 390 ± 5 to 420 ± 5 ppmv, accounting for 64% of all of the data. Carbon dioxide mixing ratio above 440 ± 5 ppmv intervals accounts for less than 10% of all data. The monthly maximum frequency interval varied

Table 1
The main 19 harmonics with the largest power spectrums of CO_2 record.

Period		Description	Power spectrum (ppmv)	Phase (°)
(Hour)	(Day)			
16,384 (2^{14})	683	Inherent cycles of FFT, seasonal, inter-annual cycle	15.1	8
8192 (2^{13})	341		16.5	−77
5461	228		6.8	179
4096 (2^{12})	171		5.5	−0.5
3277	137		5.7	−93
2048 (2^{11})	85	Atmospheric low-frequency oscillation/intra-seasonal oscillation	2.7	−62
1489	62		2.8	−88
1170	49		3.1	−15
780	33		2.8	−147
309	13	Quasi-biweekly oscillation	3.4	−127
176	7	Weekly cycle	2.8	102
174	7		2.9	−51
172	7		2.8	177
24	1	Diurnal cycle	2.6	−166
24	1		4.8	102
24	1		5.3	8
24	1		3.4	−87
12	0.5	Semi-diurnal cycle	3.8	26
12	0.5		3.1	−64

with the season, from 420 ± 5 ppmv in January to 380 ± 5 ppmv in September.

To illustrate the nature of the monthly variation of CO_2 mixing ratio, the mean values and the 10th, 25th, 50th, 75th, and 90th percentiles have been calculated and portrayed in Fig. 4. There are several things to be noted about the results. Firstly, the monthly mean value decreased from the maximum of 425.0 ppmv in January to the minimum of 381.9 ppmv in September, then increased steadily until December. This seasonal trend with a trough in the turn of summer and autumn has also been observed at other urban and background sites in the Northern Hemisphere due to the vegetation absorption of CO_2 for plant growth (Thoning and Tans, 1989; Nasrallah et al., 2003; Lintner et al., 2006; Miyaoka et al., 2007).

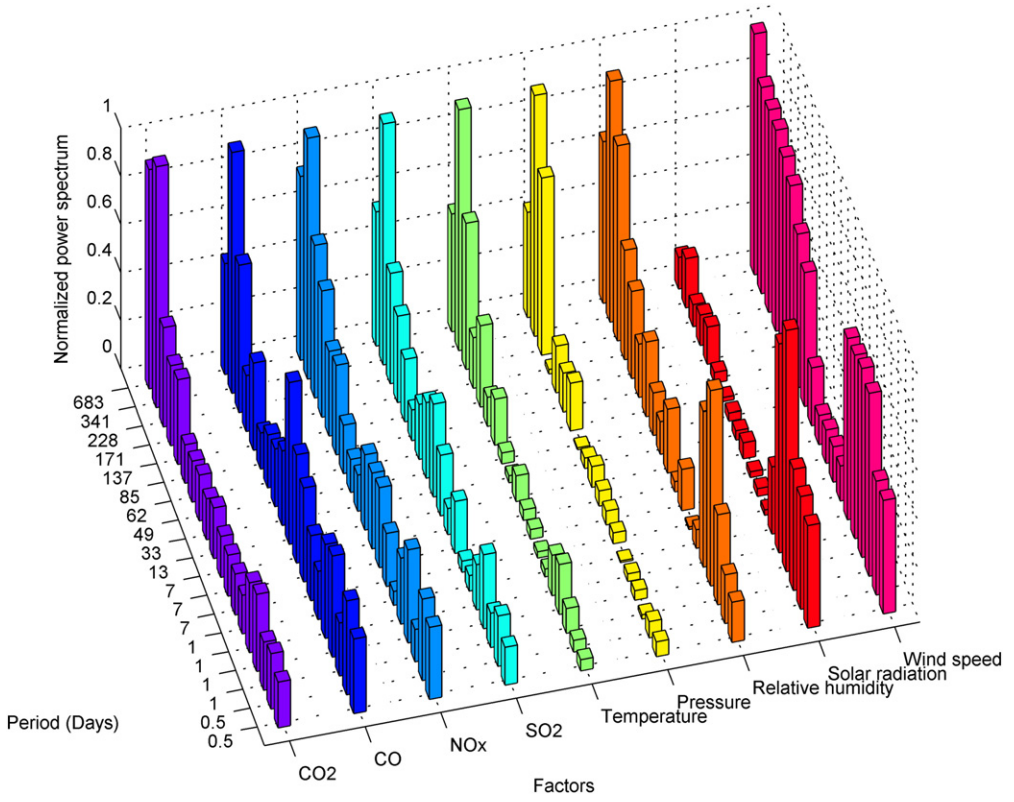

Fig. 6. Normalized power spectrum of the related factors at the same timescales, including CO_2, CO, NO_x, SO_2, temperature, pressure, relative humidity, solar radiation, and wind speed.

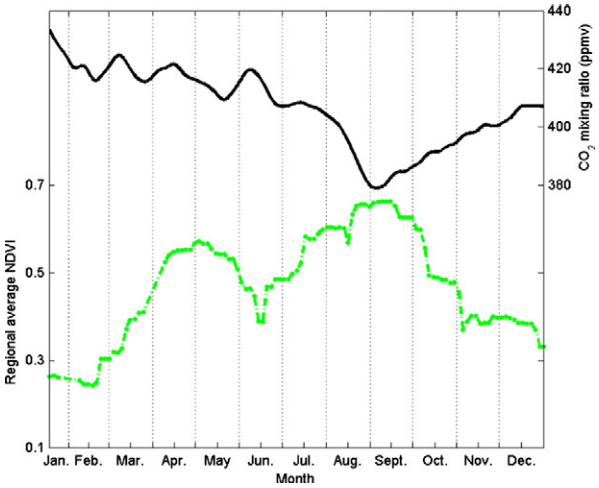

Fig. 7. The regional average values of NDVI in the area of 3.0° lattice centered at the Gulou Site, and the 30-day moving average CO_2 mixing ratio in Nanjing over 2011.

Secondly, the difference between the 25th and 75th percentiles ranged from 13.9 ppmv to 22.1 ppmv. The difference was kept steady from 4.3 ppmv to 10.2 ppmv between the 10th and 25th percentiles, but ranged largely from 7.5 ppmv to 16.8 ppmv between the 75th and 90th percentiles. Thus, the mean value was always higher than the median value in each month, with the largest difference of 5.7 ppmv in December. It indicates the frequency of high value events. Thirdly, the monthly mean value showed a decline in fluctuation from January to September, compared with the smooth upward trend from September to December.

3.2. Signals and possible explanations

The record of CO_2 in Nanjing is a combination of a yearly cycle and multiple short-term variations. In order to explore the potential impact of circulation variability on the atmospheric CO_2, the widely used filtering technique called fast Fourier transform (FFT) algorithm (Duhamel and Vetterli, 1990) was employed to partition the CO_2 record into different cycle components. To explore the role of anthropogenic emissions and meteorological condition impacts at different frequencies, the same processing was also employed on multiple data sources including air pollution components and meteorological factors.

The preprocessing has been done before FFT converting. Firstly, gaps were filled by linear interpolation as the FFT algorithm requires the data to be spaced equally in time. A total of 8352 (348 days) points were used, of which 2.11% were interpolated. The gap length ranged from 1 h to around 2 days. As the percentage of the absent data was so small, the influence on the single-sided amplitude with a different interpolation method was less than 0.4 ppmv. Secondly, the mean trend was removed from the data in order to keep it approximately centered on zero. Thirdly, the FFT algorithm was applied to convert the anomalies into the frequency domain and separate the features of interest (Thoning and Tans, 1989).

According to the power spectrum of the record presented in Fig. 5, the most significant 19 harmonic terms with the single-sided amplitude spectrums larger than a manual threshold of 2.5 ppmv are summarized in the order of timescale in Table 1. The record was decomposed into a series of harmonic terms including the seasonal, intra-seasonal, quasi-biweekly, weekly, diurnal, and semi-diurnal cycles. The superposition of the 19 harmonics can reflect the temporal variation well compared with the observation ($R = 0.72$, $n = 8352$) in Fig. 5. The combination of the first harmonics exhibits the seasonal variation of the atmospheric CO_2 observed in Nanjing. The short-term fluctuations are important phenomena in meso-scale areas, which by contrast, should be removed from the measurements at the global scale (Thoning and Tans, 1989). The intra-seasonal and quasi-biweekly cycles manifest the influence of the atmospheric circulation mechanisms. It should be noticed that there are multiple weekly, diurnal, and semi-diurnal harmonics with different phases which stand for the different influencing factors of the same timescale. The amplitudes stand for the strengths of different cycles, of which the seasonal variation is the most significant and the strengths of short-term cycles are comparable to each other.

The single-sided amplitude spectrums of the possible influencing factors were normalized for comparison as shown in Fig. 6 at the same timescales with those shown in Table 1. These peaks stand for the main harmonics which can describe the fundamental cycles of each factor. The seasonal cycles of all of them except solar radiation were significant, exhibiting the profound inherent seasonal variability. Meteorological factors including pressure, temperature, relative humidity, and wind speed present significant normalized power spectrums of intra-seasonal cycles reflecting the atmospheric low-frequency oscillation. The weekly cycles are the weakest among all the cycles of wind speed compared with the higher ones of CO and NO_x, indicating that the weekly cycles are associated with anthropogenic activities. Both the air quality indicators and the meteorological factors have significant diurnal and semi-diurnal cycles.

3.3. Influence of terrestrial biosphere

The seasonal trend observed at background stations including Lin'an (YRD), Mt. Waliguan (central Eurasian continent) (Fang et al., 2014), and Mauna Loa (global) (Tans, NOAA/ESRL) all showed a profound trough around late summer. The NDVI is an important indicator of the phase of the terrestrial biologic processes, often used to analyze the CO_2 variation caused by vegetation (Fung, 1987; Gong et al., 2011). Fig. 7 presents a comparison of the regional average NDVI with the 30-day moving average CO_2 mixing ratio over 2011. There was a significant negative correlation between them. The maximum of atmospheric CO_2 was in correspondence to the lowest NDVI in January. The CO_2 mixing ratio fell to the minimum at the turn of summer and autumn in correspondence to the occurrence of the highest NDVI during the year. The atmospheric CO_2 started increasing again accompanied by the plant senescence in autumn with weaker capability of CO_2 uptake and shorter daytime. The agreement of the phases was also observed in other zones in the Northern Hemisphere (Fung, 1987; Gong et al., 2011). The seasonal trend of atmospheric CO_2 was in good relationship with the vegetation variation and more likely influenced by the large-scale vegetation cover.

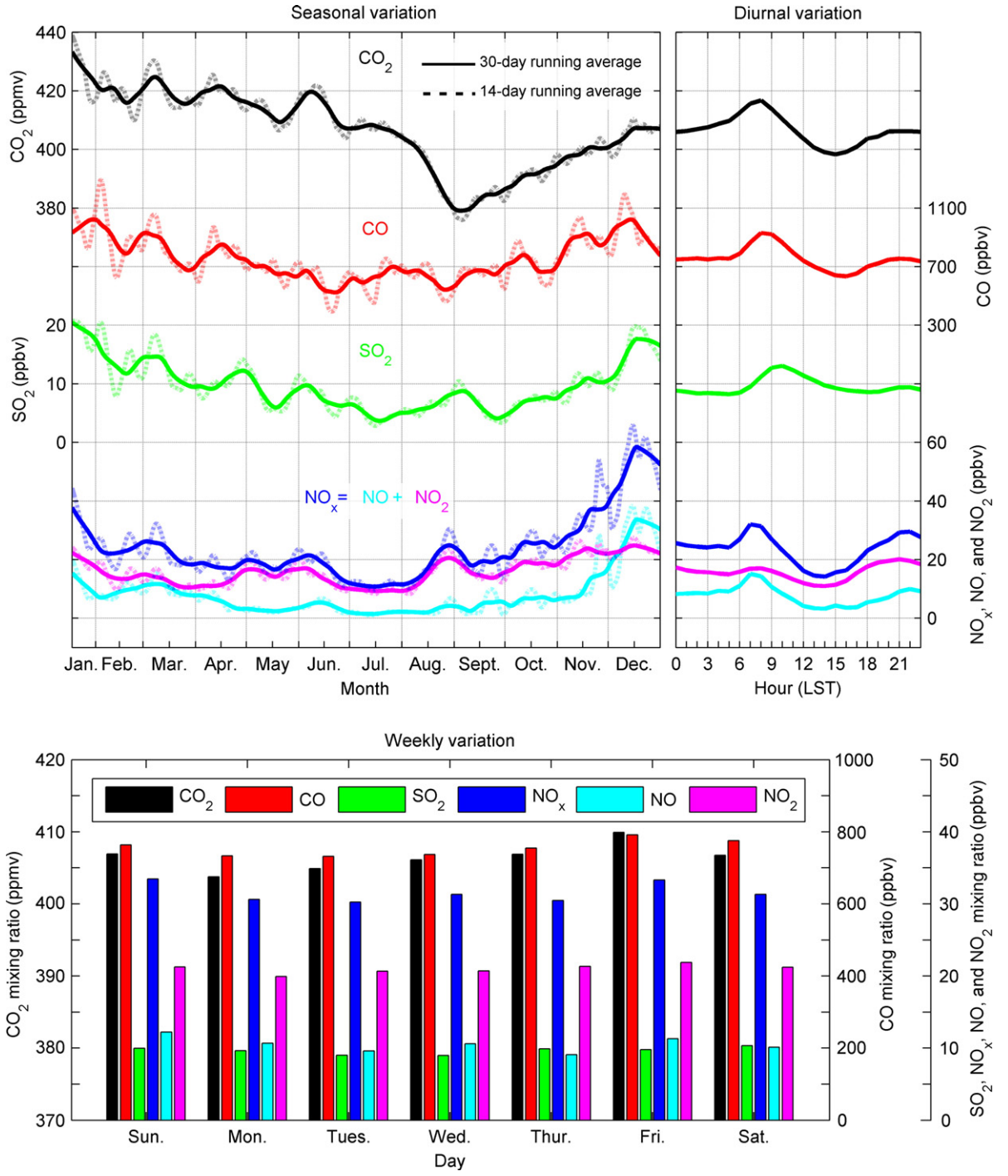

Fig. 8. The 30-day and 14-day moving average mixing ratios, the weekly and diurnal cycles of CO_2 and the concurrent air pollution components including CO, SO_2, NO_x, NO_2, and NO observed in Nanjing over 2011. Local Standard Time (Beijing time) is +8 h different from UTC time.

3.4. Influence of anthropogenic sources and meteorological conditions

3.4.1. Comparison with other gaseous pollutants

The air pollution components have often been used as indicators of CO_2 released from anthropogenic activities (Henninger and Kuttler, 2010). Fig. 8 presents the seasonal trend of 30-day running average weekly and the diurnal cycle of CO_2 and concurrent air pollution components including CO, SO_2, NO_x, NO, and NO_2 observed in Nanjing over 2011. The seasonal pattern of CO_2 showed a significant positive correlation with other air pollutants, especially from January to June and from

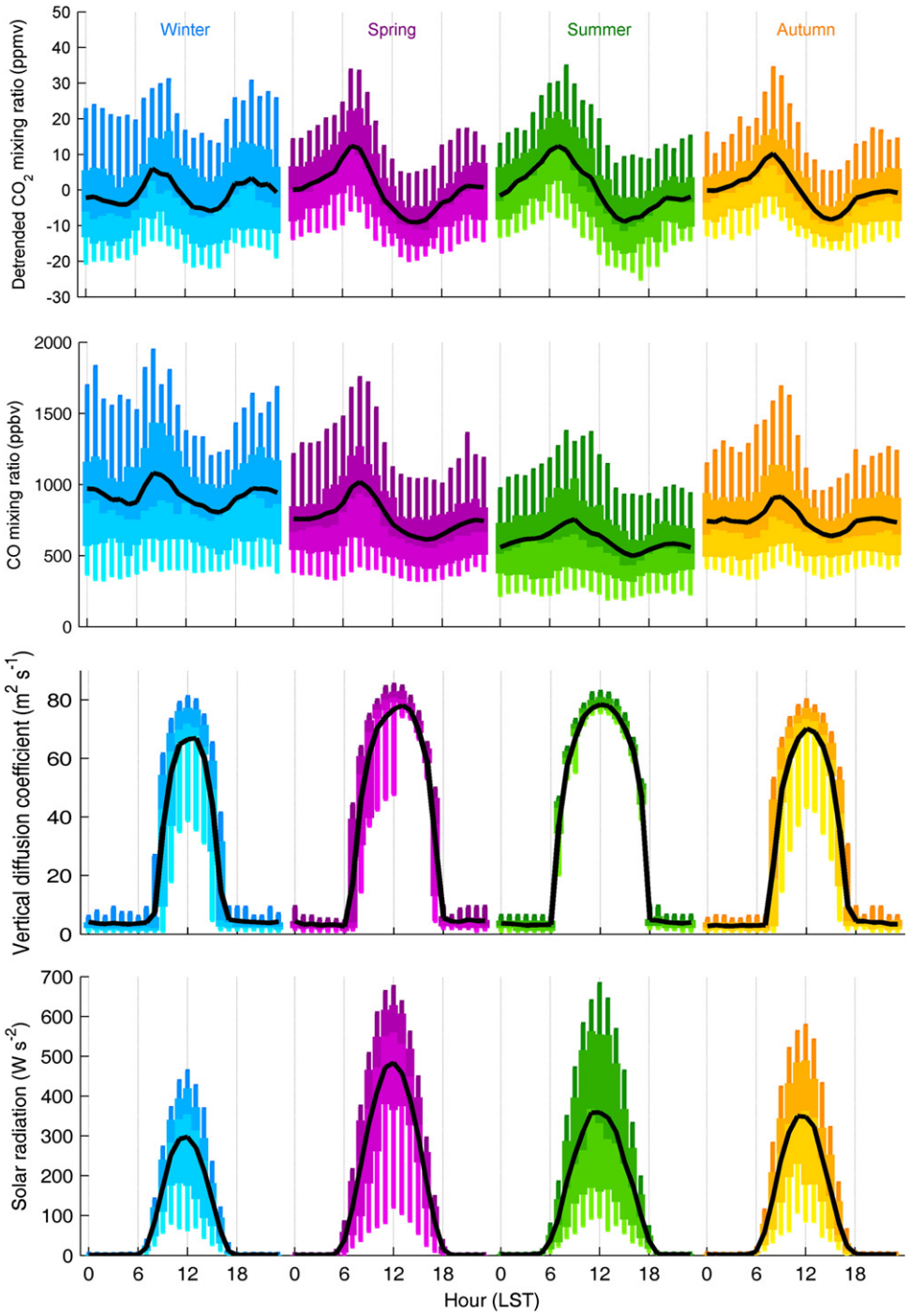

Fig. 9. Diurnal cycles of deseasonalized CO_2 and CO mixing ratios, vertical diffusion coefficient, and solar radiation with the mean values (the black lines) and the 10th, 25th, 50th, 75th, and 90th percentiles in different seasons over 2011.

late September to December. The consistent peaks and troughs of all the air components were likely caused by the movement and evolution of synoptic systems. During winter, spring, and autumn, when the plants were growing slowly or were in senescence, the trend of CO_2 was dominated by anthropogenic activities associated with the large-scale synoptic systems.

The diurnal variation of atmospheric CO_2 in Nanjing exhibits a primary peak occurring at around 0800 LST (Local Standard Time), with the hourly average mixing ratio yielding 417 ppmv, which reflects the anthropogenic emissions during rush hours. There was a trough with the mean value of 398 ppmv at 1500 LST as a result of an efficient dilution

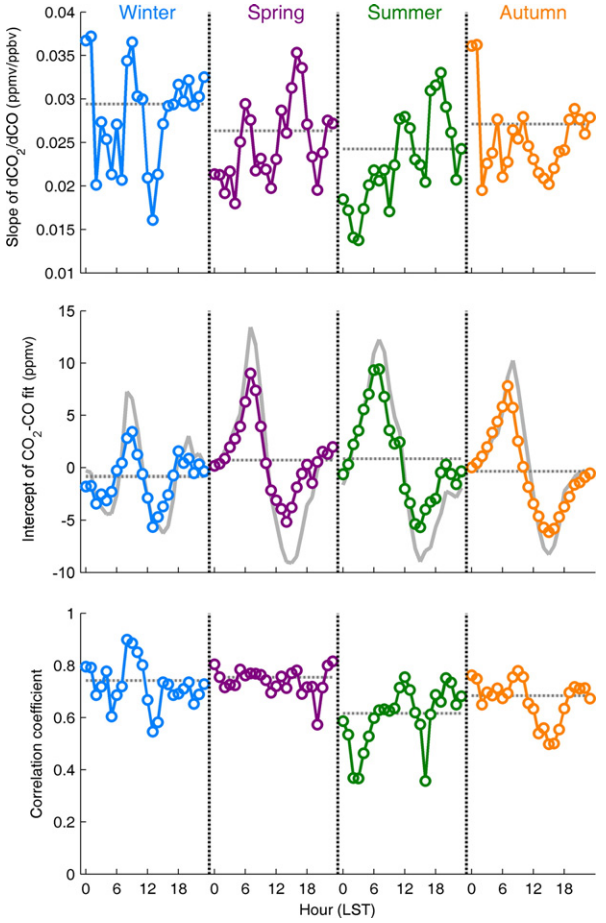

Fig. 10. The correlation slope, intercepts, and correlation coefficients of deseasonalized CO_2–CO regression at the Gulou Site, Nanjing in different seasons, 2011. The horizontal gray dashed lines stand for the seasonal average. The gray solid lines stand for the mean diurnal variation of deseasonalized CO_2.

condition by the increasing mixing layer height and the uptake of CO_2 by photosynthesis. The second largest peak appeared at around 2000 LST due to the comprehensive effect of traffic emissions, the decrease of turbulence, and the nocturnal plant respiration. This peak declined slowly until the predawn hours.

The weekly variation of CO_2 showed an amplitude of 6 ppmv with a minimum on Monday which then increasing slowly to a maximum on Friday. The mixing ratio then decreased to a minimum again when weekend ends. The air quality indicators CO and NO_2 shared a similar weekly cycle. Traffic emission is an important source of gaseous components in YRD (Kang et al., 2013). This pattern is assumed mainly due to the accumulative contribution of anthropogenic emissions during the weekdays.

3.4.2. CO_2–CO relationship

As a product of inefficient combustion, CO has been taken as a tracer of CO_2 from combustion. The CO_2/CO ratio and the CO_2–CO correlation slope provide the information about the release of CO_2 from anthropogenic activities (Tsutsumi et al, 2006; Miyaoka et al., 2007; Wang et al., 2010b; Zhang et al., 2013). In order to gain a better insight into anthropogenic influence, the CO_2 mixing ratio was deseasonalized by removing the seasonal trend of 30-day running average. Fig. 9 presents the diurnal cycles of deseasonalized CO_2, CO, the vertical diffusion coefficient, and solar radiation in different seasons over 2011. The deseasonalized CO_2 followed a bimodal mean diurnal pattern in winter, and a sinusoidal one in the other three seasons. During the winter season, there were two comparable peaks exhibited at 0800 and 2000 LST spaced by two troughs before dawn and in the afternoon with the mean diurnal amplitude of 15 ppmv. During the other three seasons, the sinusoidal pattern showed a major peak at around 0800 LST and a profound trough at around 1500 LST with the mean diurnal amplitude of around 22 ppmv, 21 ppmv, and 18 ppmv, respectively. The mean diurnal pattern of CO was in phase with that of CO_2, which indicates strong influences of combustion on CO_2 indicating that anthropogenic emissions play an important role in the diurnal variation of CO_2.

The eddy diffusion coefficient or eddy diffusivity is a parameter used to quantify the eddy diffusion process in the atmosphere. The calculated vertical diffusion coefficient (Businger et al., 1971; Carl et al., 1973) exhibited a well-mixed atmosphere during the daytime in all the seasons with the maxima at noon mainly due to the solar zenith angle. The width of the peak narrowed in cold seasons and broadened in warm seasons due to the time of sunrise and sunset. The diffusion coefficient decreased before the evening rush hour, causing a weak vertical mixing, which led to a shallow trough in the afternoon and a secondary peak in the evening during winter.

Different from CO_2, the diurnal amplitude of CO in summer was not as large as that in spring. This can be explained by the strong effect of the respiration process during nighttime and the photosynthesis process during daytime by vegetation. The maxima of solar radiation all over the year appeared in spring and summer. Combined with the NDVI shown in Fig. 7, the photosynthesis process under the condition of sufficient solar radiation was responsible for the lower CO_2 mixing ratio during the day, which led to a profound trough of atmospheric CO_2 in the afternoon and formed the large diurnal amplitude during the plant growing season.

The maxima of CO_2 mixing ratio had a high coherence with those of CO especially in December, exhibiting the homology of the anthropogenic sources. To distinguish between the accumulative contributions of biospheric activities during growing seasons and anthropogenic emissions to CO_2, the correlation analysis was modified for comparison by removing the seasonal trend of 30-day running average from both CO_2 and CO. The correlation coefficients between CO_2 and CO before and after deseasonalization were 0.56 and 0.62 ($n = 8062$), respectively. The overall CO_2/CO correlation slope before and after deseasonalization at the Gulou Site was about 0.0272 ppmv/ppbv and 0.0265 ppmv/ppbv, respectively during 2011, a little higher than that of 0.024 ppmv/ppbv observed at Miyun, Beijing during 2007–2008 (Wang et al., 2010b), whereas the emission ratio of fossil fuel combustion is 0.026 ppmv/ppbv in China (Suntharalingam et al., 2004), indicating that the source of CO_2 in Nanjing is mainly fossil fuel combustion.

The relationship between deseasonalized CO_2 and CO including CO_2/CO correlation slope, intercept, and correlation coefficient in different seasons is shown in Fig. 10. The seasonal average correlation slope varied from 0.024 ppmv/ppbv in summer to 0.029 ppmv/ppbv in winter. The diurnal pattern of correlation slope appeared with irregular peaks and troughs in

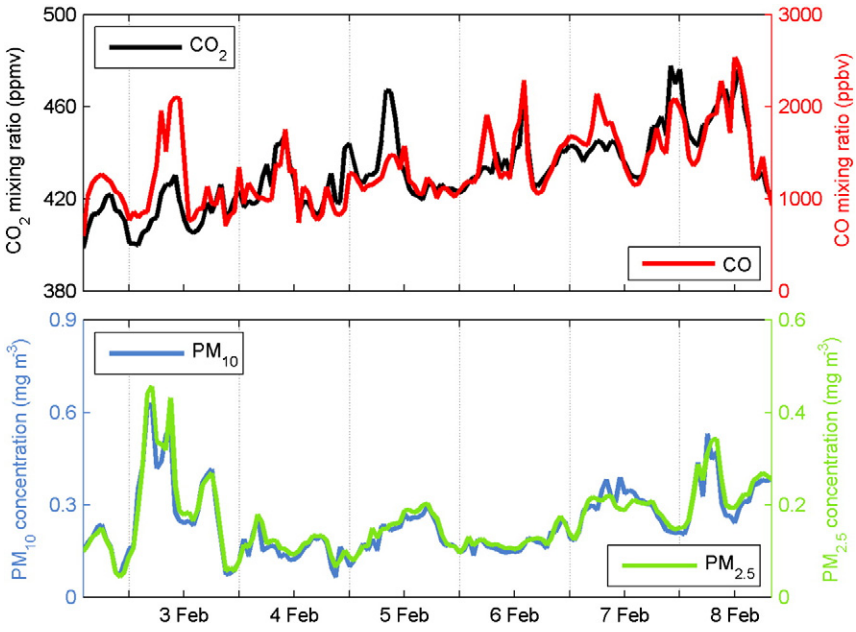

Fig. 11. Time series of CO_2, CO, PM_{10}, and $PM_{2.5}$ observed during the Spring Festival holiday in 2011 in urban Nanjing.

all the seasons, which is quite different from the observation at rural sites (Wang et al., 2010b), indicating large quantities of random emissions from anthropogenic activities in urban areas. The intercept reflects the ideal CO_2 variation under non-CO condition. The diurnal amplitude was smaller in winter than in other three seasons, indicating the weakest photosynthesis and respiratory processes by plants in winter. This is different from the constant pattern observed in a northerner area (Wang et al., 2010b) with much fewer evergreens in winter. By contrast, the intercept shows a similar pronounced diurnal cycle in spring, summer, and autumn, with a peak at 7 a.m. and a trough at 14–15 p.m. local time. This reflects the strong effect of vegetation absorbing CO_2 through the photosynthesis process in the daytime and releasing it through the respiration process at night. The diurnal variation of intercepts was similar to the mean diurnal pattern of CO_2, but with smaller amplitude. The reduction of diurnal amplitude varied from 4 ppmv to 8 ppmv. This reflects the influence of anthropogenic emissions under the seasonally varying meteorological conditions.

There were some high CO_2 episodes observed during the study period. Take the case that occurred in the Spring Festival holiday for example as shown in Fig. 11. The Spring Festival (or the Chinese New Year) holiday is a period when large quantities of fireworks are set, which thus leads to air pollutions and large emissions of carbonaceous gases and aerosols (Feng et al., 2012). The mixing ratio of CO_2 was much higher than the annual mean value, as well as the CO, PM_{10}, and $PM_{2.5}$. The trend of CO_2 and CO matched quite well with the CO_2/CO correlation slope of 0.034 ppmv/ppbv, which is about 25%–30% higher than the average fossil fuel emission ratio. This indicates high efficiency of combustion, and firework setting is one of the main sources of CO_2 during the Spring Festival holiday.

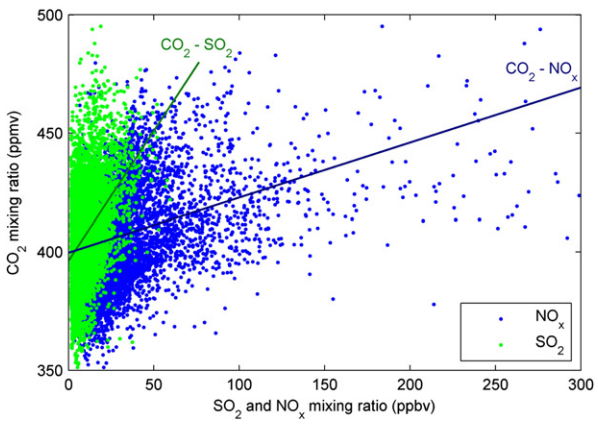

Fig. 12. The CO_2–SO_2 and CO_2–NO_x relationships observed at Nanjing over 2011.

3.4.3. CO_2–SO_2 and CO_2–NO_x relationships

Both SO_2 and NO_x are reactive chemical components and can be representative of local air quality. As the YRD region is heavily industrialized, highly urbanized and densely populated, anthropogenic emissions in this area are very large. In order to separate the contributions from coal combustion and motor vehicle emissions, the CO_2–SO_2 and CO_2–NO_x relationships observed in Nanjing over 2011 were investigated as shown in Fig. 12. The correlation coefficients of CO_2–SO_2 and CO_2–NO_x were 0.41 and 0.34, respectively, both with high significance. The correlation slopes of CO_2/SO_2 and CO_2/NO_x were 1.10 ppmv/ppbv and 0.23 ppmv/ppbv, respectively. The intercept of CO_2/SO_2 was about 3 ppmv lower than that of CO_2/NO_x. Multiyear inventories showed that vehicular and industrial CO_2 emissions have substantially increased in China, especially in economically developed areas including the YRD region (Wang et al., 2010a; Liu et al., 2013). According to the vehicle emission inventory of Nanjing, the estimated CO_2/CO of vehicle emission was about

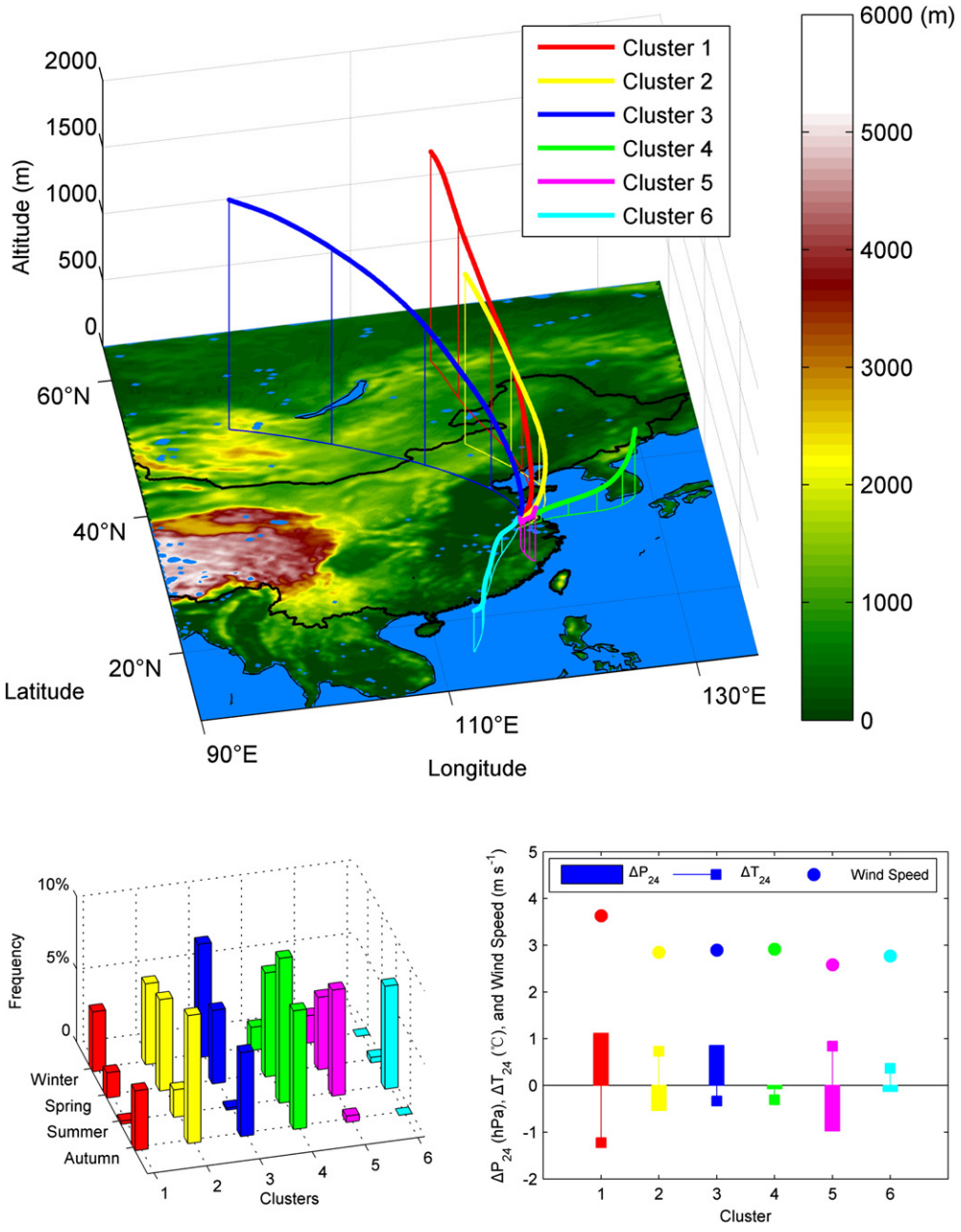

Fig. 13. Clusters of 5-day backward trajectories arriving at the Gulou Site in Nanjing during the study period by the HYSPLIT model, with calculated seasonal frequencies, surface meteorological observations including the 24 h surface allobaric change (ΔP_{24}, hPa), the 24 h air temperature change (ΔT_{24}, °C), and the surface wind speed ($m\ s^{-1}$). In the figure of trajectories, the vertical fine lines of each cluster stand for the intervals of the 5 days.

0.096 ppmv/ppbv, which was much higher than that of 0.024–0.029 ppmv/ppbv mentioned in the previous section calculated with the observed hourly CO_2 and CO data in Nanjing. These all indicate that coal combustion contributes more to the emission of CO_2 than motor vehicles at long-term timescale.

3.5. Synoptic air mass trajectories

The backward trajectories can be used to help understand transport paths and identify source regions of air masses (Fleming et al., 2012). The 1391 5-day backward trajectories were classified into 6 groups based on cluster analysis by the HYSPLIT model as shown in Fig. 13 with corresponding surface meteorological observations, and the interval of each day on each trajectory is divided by vertical fine lines. The backward trajectories were affected by the movement of synoptic systems. Thus the clusters of backward trajectories also indicate major synoptic systems. Clusters 1 and 3 were representative of fast moving air masses that originated from remote Siberia and Mongolia. These cold air parcels were driven by the Mongolian high pressure that frequently occurred in cold seasons, with positive surface pressure change and negative air temperature

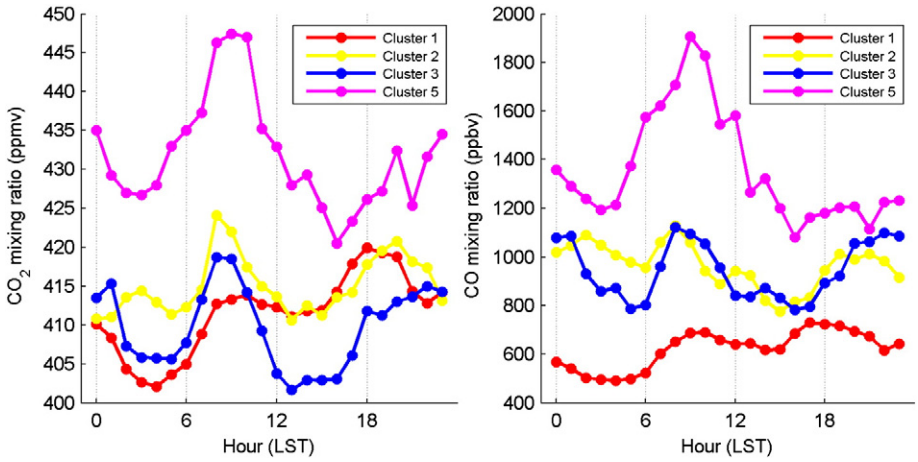

Fig. 14. The diurnal pattern of CO_2 and CO mixing ratios in some clusters of backward trajectories in winter (DJF).

change observed in Nanjing. Air masses in Cluster 1 were the driest and strongest among these 6, transporting along the longest pathway and bringing the largest surface wind speed, indicating a cold front. Cluster 2 stood for mild air masses from Northern China via Bohai Bay, reflecting low pressure system with negative surface allobaric pressure change and positive temperature change. Cluster 4 with the largest frequency consisted of the wettest air parcels that originated from the Korean Peninsula passing over eastern seas, showing uniform pressure field. Cluster 5 presented the local air masses coming from the nearest source region in the South, which often occurred in warm seasons, under the control of strong low pressure system with the smallest observational surface wind speed. Cluster 6 included wet air parcels starting from the South China Sea traveling along Southern China, mainly occurring in summer with a uniform pressure field driven by the Summer Monsoon.

Considering the relatively long lifetime of CO_2 and CO in winter, the low frequencies of Clusters 4 and 6 in the cold season, and the low variation of the clusters of trajectories, the diurnal patterns of CO_2 and CO mixing ratios for the other 4 clusters in winter were calculated as exhibited in Fig. 14. The diurnal patterns of CO_2 and CO for each cluster were similar. Comparing the CO_2 and CO mixing ratios at a restricted time of day when mixing is strong (e.g. around 15 p.m.), the largest CO_2 mixing ratio over 420 ppmv combined with the highest CO over 1000 ppbv appeared in Cluster 5 of local air masses. High CO_2 episodes such as the severe air pollution period during the Spring Festival mentioned in the previous section were included in Cluster 5. It indicates that local anthropogenic emissions are the main source of CO_2 in the study area. Air mass in Clusters 1 and 2 showed a CO_2 mixing ratio of around 410 ppmv probably due to the transport path via the Northern China Plain which is also considered as a large anthropogenic source (Gregg et al., 2008; Wang et al., 2010b; Sun et al., 2013). With the same fast continental air flow driven by a cold high-pressure system, the air mass in Cluster 3 showed relatively low CO_2 mixing ratio of 403 ppmv.

4. Summary and conclusions

We have analyzed temporal variations of atmospheric CO_2 observed at Gulou, an urban site in Nanjing over 2011. This site is located almost in the center of Nanjing, thus it can reflect major characteristics of atmospheric components in the urban area. Several conclusions can be drawn from the comprehensive analysis during the campaign. The annual average mixing ratio of CO_2 was 406.5 $\pm$ 20.0 ppmv with about 64% of the measurements ranging from 385 ppmv to 425 ppmv. The CO_2 record had multiple signals which were caused by different sources and sinks or meteorological conditions. The CO_2 mixing ratio showed significant signals at different timescales including seasonal, intra-seasonal, quasi-biweekly, weekly, diurnal, and semi-diurnal cycles by the FFT algorithm, which were also exhibited in the signal analysis of air pollution components and meteorological factors. The seasonal, intra-seasonal, and quasi-biweekly cycles were mainly caused by the atmospheric oscillations at different timescales. The anthropogenic activities were a main reason for the short-term variations of CO_2. The weekly cycle was weaker than seasonal and diurnal ones and was mainly caused by the traffic emissions. Fossil fuel combustion was the main anthropogenic source of CO_2 in the urban area with the CO_2/CO correlation slope varying from 0.024 ppmv/ppbv to 0.029 ppmv/ppbv, in which coal combustion contributed more than motor vehicle emission. The clustered backward trajectories showed that the local anthropogenic emissions contributed the most to the high CO_2 in the urban area through atmospheric transportation.

Acknowledgments

This work was supported by the National Key Basic Research Program of China (2010CB950704, 2014CB441203, and 2010CB428503), the Young Scientist Fund of the National Natural Science Foundation of China (41205111), the Fundamental Research Funds for the Key Universities (1127020701), the FP7 project: REQUA (PIRSES-GA-2013-612671), and the fund for the Priority Academic Program Development of

Jiangsu Higher Education Institutions (PAPD). We are sincerely grateful for the NDVI products provided by JAXA/NIES/MOE (http://www.jaxa.jp/projects/sat/gosat/index_e.html) and gratefully acknowledge the NOAA Air Resources Laboratory (ARL) for the provision of the HYSPLIT transport and dispersion model and/or READY website (http://www.ready.noaa.gov).

References

Artuso, F., Chamard, P., Piacentino, S., et al., 2009. Influence of transport and trends in atmospheric CO_2 at Lampedusa. Atmos. Environ. 43, 3044–3051. http://dx.doi.org/10.1016/j.atmosenv.2009.03.027.

Boden, T.A., Marland, G., Andres, R.J., 2010. Global, regional, and national fossil-fuel CO_2 emissions. Carbon Dioxide Information Analysis Center, Oak Ridge National Laboratory, U.S. Department of Energy, Oak Ridge, Tenn., U.S.A. http://dx.doi.org/10.3334/CDIAC/00001_V2010.

Businger, J.A., Wyngaard, J.C., Izumi, Y., et al., 1971. Flux–profile relationship in the atmospheric surface layer. J. Atmos. Sci. 28, 181–189. http://dx.doi.org/10.1175/1520-0469(1971)028<0181:FPRITA>2.0.CO;2.

Butler, J.H., Montzka, S.A., 2013. The NOAA Annual Greenhouse Gas Index (AGGI). NOAA/ESRL Global Monitoring Division, (summer, http://www.esrl.noaa.gov/gmd/aggi/aggi.html).

Carl, D.M., Tarbell, T.C., Panofsky, H.A., 1973. Profiles of wind and temperature from towers over homogeneous terrain. J. Atmos. Sci. 30, 788–794. http://dx.doi.org/10.1175/1520-0469(1973) 030<0788:POWATF>2.0.CO;2.

Draxler, R.R., Rolph, G.D., 2013. HYSPLIT (HYbrid Single-Particle Lagrangian Integrated Trajectory) Model Access Via NOAA ARL READY Website(http://www.arl.noaa.gov/HYSPLIT.php) NOAA Air Resources Laboratory, College Park, MD.

Duhamel, P., Vetterli, M., 1990. Fast Fourier transforms: a tutorial review and a state of the art. Signal Process. 19, 259–299.

Fang, S., Zhou, L., Tans, P., et al., 2014. In situ measurement of atmospheric CO_2 at the four WMO/GAW stations in China. Atmos. Chem. Phys. 14, 2541–2554. http://dx.doi.org/10.5194/acp-14-2541-2014.

Feng, J., Sun, P., Hu, X., et al., 2012. The chemical composition and sources of $PM_{2.5}$ during the 2009 Chinese New Year's holiday in Shanghai. Atmos. Res. 118, 435–444. http://dx.doi.org/10.1016/j.atmosres.2012.08.012.

Ferrarese, S., Longhetto, A., Cassardo, C., et al., 2002. A study of seasonal and yearly modulation of carbon dioxide sources and sinks, with a particular attention to the Boreal Atlantic Ocean. Atmos. Environ. 36, 5517–5526. http://dx.doi.org/10.1016/S1352-2310(02)00669-6.

Finlayson-Pitts, B.J., Pitts Jr., J.N., 2000. Chemistry of the Upper and Lower Atmosphere: Theory, Experiments and Applications. Academic Press, New York.

Fleming, Z., Monks, P., Manning, A., 2012. Review: untangling the influence of air-mass history in interpreting observed atmospheric composition. Atmos. Res. 104–105, 1–39. http://dx.doi.org/10.1016/j.atmosres.2011.09.009.

Fung, I.Y., 1987. Application of Advanced Very High Resolution Radiometer vegetation index to study atmosphere–biosphere exchange of CO_2. J. Geophys. Res. Atmos. 92 (D3), 2999–3015. http://dx.doi.org/10.1029/JD092iD03p02999.

García, M., Sanchez, M., Pérez, I., 2012. Differences between carbon dioxide levels over suburban and rural sites in Northern Spain. Environ. Sci. Pollut. Res. 19, 432–439. http://dx.doi.org/10.1007/s11356-011-0575-4.

Gong, C.L., Zhou, Y., Hu, Y., 2011. Analyzing the CO_2 column amount in China with GOSAT data. Proc. SPIE8193, International Symposium on Photoelectronic Detection and Imaging 2011: Advances in Infrared Imaging and Applications, p. 819327 http://dx.doi.org/10.1117/12.900295.

Gorka, M., Lewicka-Szczebak, D., 2013. One-year spatial and temporal monitoring of concentration and carbon isotopic composition of atmospheric CO_2 in a Wrocław (SW Poland) city area. Appl. Geochem. 35, 7–13. http://dx.doi.org/10.1016/j.apgeochem.2013.05.010.

Gratani, L., Varone, L., 2005. Daily and seasonal variation of CO_2 in the city of Rome in relationship with the traffic volume. Atmos. Environ. 39, 2619–2624. http://dx.doi.org/10.1016/j.atmosenv.2005.01.013.

Gregg, J.S., Andres, R.J., Marland, G., 2008. China: emissions pattern of the world leader in CO_2 emissions from fossil fuel consumption and cement production. Geophys. Res. Lett. 35, L08806. http://dx.doi.org/10.1029/2007GL032887.

Henninger, S., Kuttler, W., 2010. Near surface carbon dioxide within the urban area of Essen, Germany. Phys. Chem. Earth 35, 76–84. http://dx.doi.org/10.1016/j.pce.2010.03.006.

Hofmann, D.J., Butler, J.H., Tans, P.P., 2009. A new look at atmospheric carbon dioxide. Atmos. Environ. 43, 2084–2086. http://dx.doi.org/10.1016/j.atmosenv.2008.12.028.

Houghton, R.A., 2010. How well do we know the flux of CO_2 from land-use change? Tellus 62B, 337–351. http://dx.doi.org/10.1111/j.1600-0889.2010.00473.x.

Houghton, R.A., van der Werf, G.R., DeFries, R.S., et al., 2012. Regional carbon cycle assessment and processes (RECCAP) synthesis chapter G2: carbon emissions from land use and land-cover change. Biogeosci. Discuss. 9, 835–878. http://dx.doi.org/10.5194/bg-9-5125-2012.

Idso, C.D., Idso, S.B., Balling Jr., R.C., 2001. An intensive two-week study of an urban CO_2 dome in Phoenix, Arizona, USA. Atmos. Environ. 35, 995–1000. http://dx.doi.org/10.1016/S1352-2310(00)00412-X.

Idso, S.B., Idso, C.D., Balling Jr., R.C., 2002. Seasonal and diurnal variations of near-surface atmospheric CO_2 concentration within a residential sector of the urban CO_2 dome of Phoenix, AZ, USA. Atmos. Environ. 36, 1655–1660. http://dx.doi.org/10.1016/S1352-2310(02)00159-0.

Jiang, F., Wang, H., Chen, J., et al., 2013. Nested atmospheric inversion for the terrestrial carbon sources and sinks in China. Biogeosciences 10, 5311–5324. http://dx.doi.org/10.5194/bg-10-5311-2013.

Kang, H., Zhu, B., Su, J., et al., 2013. Analysis of a long-lasting haze episode in Nanjing, China. Atmos. Res. 120–121, 78–87. http://dx.doi.org/10.1016/j.atmosres.2012.08.004.

Keeling, C.D., Bacastow, R.B., Bainbridge, A.E., et al., 1976. Atmospheric carbon dioxide variations at Mauna Loa Observatory, Hawaii. Tellus 28 (6), 538–551. http://dx.doi.org/10.1111/j.2153-3490.1976.tb00701.x.

Liao, J., Wang, T., Wang, X., et al., 2014. Impacts of different urban canopy schemes in WRF/Chem on regional climate and air quality in Yangtze River Delta, China. Atmos. Res. 145–146, 226–243. http://dx.doi.org/10.1016/j.atmosres.2014.04.005.

Lintner, B.R., Buermann, W., Koven, C.D., et al., 2006. Seasonal circulation and Mauna Loa CO_2 variability. J. Geophys. Res. 111 (D13104). http://dx.doi.org/10.1029/2005JD006535.

Liu, M., Wang, H., Wang, H., et al., 2013. Refined estimate of China's CO_2 emissions in spatiotemporal distributions. Atmos. Chem. Phys. 13, 10873–10882. http://dx.doi.org/10.5194/acp-13-10873-2013.

Mao, H., Talbot, R., 2004. O_3 and CO in New England: temporal variations and relationships. J. Geophys. Res. 109 (D21304). http://dx.doi.org/10.1029/2004JD004913.

Miyaoka, Y., Inoue, H., Sawa, Y., et al., 2007. Diurnal and seasonal variations in atmospheric CO_2 in Sapporo, Japan: anthropogenic sources and biogenic sinks. Geochem. J. 41, 429–436.

Nasrallah, H.A., Balling Jr., R.C., Madi, S.M., et al., 2003. Temporal variations in atmospheric CO_2 concentrations in Kuwait City, Kuwait with comparisons to Phoenix, Arizona, USA. Environ. Pollut. 121, 301–305. http://dx.doi.org/10.1016/S0269-7491(02)00221-X.

Pérez, I.A., Sánchez, M.L., García, M.A., et al., 2009. Daily and annual cycle of CO_2 concentration near the surface depending on boundary layer structure at a rural site in Spain. Theor. Appl. Climatol. 98, 269–277. http://dx.doi.org/10.1007/s00704-009-0112-2.

Pérez, I.A., Sánchez, M.L., García, M.A., et al., 2011. Persistence analysis of CO_2 concentrations recorded at a rural site in the upper Spanish plateau. Atmos. Res. 100 (1), 45–50. http://dx.doi.org/10.1016/j.atmosres.2010.12.025.

Pongratz, J., Caldeira, K., 2012. Attribution of atmospheric CO_2 and temperature increases to regions: importance of preindustrial land use change. Environ. Res. Lett. 7, 034001. http://dx.doi.org/10.1088/1748-9326/7/3/034001.

Rolph, G.D., 2013. Real-time Environmental Applications and Display sYstem (READY) Website(http://www.ready.noaa.gov) NOAA Air Resources Laboratory, College Park, MD.

Sahay, S., Ghosh, C., 2013. Monitoring variation in greenhouse gases concentration in Urban Environment of Delhi. Environ. Monit. Assess. 185, 123–142. http://dx.doi.org/10.1007/s10661-012-2538-8.

Song, T., Wang, Y., 2012. Carbon dioxide fluxes from an urban area in Beijing. Atmos. Res. 106, 139–149. http://dx.doi.org/10.1016/j.atmosres.2011.12.001.

Sun, Y., Zhou, X., Wai, K., et al., 2013. Simultaneous measurement of particulate and gaseous pollutants in an urban city in North China Plain during the heating period: implication of source contribution. Atmos. Res. 134 (1), 24–34. http://dx.doi.org/10.1016/j.atmosres.2013.07.011.

Suntharalingam, P., Jacob, D.J., Palmer, P.I., et al., 2004. Improved quantification of Chinese carbon fluxes using CO_2/CO correlations in Asian outflow. J. Geophys. Res. Atmos. 109 (D18S18). http://dx.doi.org/10.1029/2003JD004362.

Talbot, R., Mao, H., Sive, B., 2005. Diurnal characteristics of surface level O_3 and other important trace gases in New England. J. Geophys. Res. Atmos. 110 (D09307), 1–16. http://dx.doi.org/10.1029/2004JD005449.

Tans, P., NOAA/ESRL (www.esrl.noaa.gov/gmd/ccgg/trends/) and Keeling, R., Scripps Institution of, Oceanography (scrippsco2.ucsd.edu/); 2014 (ftp://ftp.cmdl.noaa.gov/products/trends/co2/co2_annmean_mlo.txt).

Thoning, K.W., Tans, P.P., 1989. Atmospheric carbon dioxide at Mauna Loa Observatory 2. Analysis of the NOAA GMCC data, 1974–1985. J. Geophys. Res. 94 (D6), 8549–8565. http://dx.doi.org/10.1029/JD094iD06p08549 (0148-0227/89/89JD-00315505.00).

Tsutsumi, Y., Mori, K., Ikegami, M., et al., 2006. Long-term trends of greenhouse gases in regional and background events observed during 1998–2004 at Yonagunijima located to the east of the Asian continent. Atmos. Environ. 40, 5868–5879. http://dx.doi.org/10.1016/j.atmosenv.2006.04.036.

Wang, H., Fu, L., Yu, Z., et al., 2010a. Trends in vehicular emissions in China's mega cities from 1995 to 2005. Environ. Pollut. 158, 394–400. http://dx.doi.org/10.1016/j.envpol.2009.09.002.

Wang, Y., Munger, J.W., Xu, S., et al., 2010b. CO_2 and its correlation with CO at a rural site near Beijing: implications for combustion efficiency in China. Atmos. Chem. Phys. 10, 8881–8897. http://dx.doi.org/10.5194/acp-10-8881-2010.

Zhang, F., Zhou, L.X., Conway, T.J., et al., 2013. Short-term variations of atmospheric CO_2 and dominant causes in summer and winter: analysis of 14-year continuous observational data at Waliguan, China. Atmos. Environ. 77, 140–148. http://dx.doi.org/10.1016/j.atmosenv.2013.04.067.